Mass Spectrometry

Deutsche Ausgabe: DOI: 10.1002/ange.201500906
Internationale Ausgabe: DOI: 10.1002/anie.201500906

Development of Experiment and Theory to Detect and Predict Ligand Phase Separation on Silver Nanoparticles**

Zachary Farrell, Steve Merz, Jon Seager, Caroline Dunn, Sergei Egorov, and David L. Green**

Abstract: *MALDI mass-spectrometry measurements are combined with self-consistent mean-field (SCF) calculations to detect and predict ligand phase separation on Ag nanoparticles. The experimental and theoretical techniques complement each other by enabling quantification of the nearest-neighbor distribution of a ligand mixture in a monolayer shell. By tracking a characteristic metallic fragment family, analysis of a MALDI spectrum produces a frequency distribution corresponding to specific ligand patterning. Inherent to the SCF calculation is the enumeration of local interactions that dictate ligand assembly. Interweaving MALDI and SCF facilitates a comparison between the experimentally and theoretically derived frequency distributions as well as their deviation from a well-mixed state. Thus, we combine these techniques to detect and predict phase separation in monolayers that mix uniformly or experience varying degrees of de-mixing, including microphase separation and stripe formation. Definition of MALDI removed as this is a commonly recognized technique.*

The interfacial engineering of nanoparticles is an emergent area of research that is garnering significant interest for application in areas such as optics,[1] electronics,[2] and drug delivery.[3] Thus, it is important to exert control over the interface of nanoparticles, which dictates their degree of compatibility with and assembly in soft materials,[4] provides reactive sites for attachment of molecules, such as drug payloads,[3] and tunes the surface plasmon to a wavelength of interest.[1] The starting point for interfacial modification is the self-assembled monolayer (SAM), or the layer of molecules (i.e., ligands) that form a shell around the nanoparticle. One strategy for controlling SAM properties involves the use of two or more ligands, resulting in a mixed-ligand monolayer. On interfaces where ligands can attach and detach through adsorption/desorption equilibrium or move through surface diffusion, molecular simulations indicate that the phase separation of ligands occur for those with significant physical and/or chemical differences, such as alkane thiols with a sufficient chain-length mismatch.[5] Experimentally, ensemble-based methods, such as FTIR spectroscopy, or single-nanoparticle methods, such as scanning tunneling microscopy (STM), have been used to interrogate ligand phase separation.[6] However, such ensemble-based methods typically yield semiquantitative results on mixed ligand SAMs, and STM measurements of ligand phase separation have recently been called into question.[7] Towards the advancement of single-nanoparticle methods, we have developed a complementary set of experimental and theoretical tools to probe the effects of nearest-neighbor interactions on ligand phase separation.

The experimental technique employed is MALDI mass spectrometry, an ensemble-based method which produces mass spectra of solid analytes through ionization with a UV laser, thereby accelerating analyte fragments towards a detector that typically resolves species by time-of-flight.[8] This technique has general utility for metallic nanoparticles, but we currently employ only silver (in this Communication) as well as a further study of gold (in the Supporting Information). In the case of silver, fragments are produced, which have a generic formula of $Ag_{n+1}L_n$ where n is the number of ligands (L) on a fragment with $n+1$ Ag atoms.[9] We chose to analyze the Ag_6L_5 fragment family as it was prevalent in every spectrum and its peaks provide good resolution. The parameter L represents the combination of two ligands, one being dodecanethiol (DDT) and the other being deuterated DDT [D_{25}]DDT or butanethiol (BT). Analysis of the fragment provides a representative measure of the mol% of DDT, [D_{25}]DDT, and BT on the surface and the phase separation. (For a detailed comparison of the Ag_6L_5 ion family with others, see the Supporting Information). Figure 1 shows the MALDI spectrum for the Ag_6L_5 fragment from silver nanoparticles functionalized with a 49:51 mol% mixture of adsorbed DDT and its deuterated analog [D_{25}]DDT, respectively.

Anticipating that the Ag_6L_5 fragment provides a representative sampling of the surface, it is possible to create a frequency distribution. In the case of Ag_6L_5 with dodecanethiol as one of the two ligands, it is convenient to conceptualize each of the six possible ions in terms of how many DDT are present in each fragment (i.e., 0–5 ligands). Knowledge of the frequency distribution also facilitates the computation of the relative amounts of each ligand, enabling a calculation of the binomial distribution, indicative of random ligand mixing. By comparison of the experimental frequency distribution with the binomial distribution in Equation (2) (discussed below) it is possible to calculate a sum-of-squares residual (SSR), which is representative of

[*] Z. Farrell, S. Merz, C. Dunn, Dr. D. L. Green
University of Virginia, Department of Chemical Engineering
Charlottesville, VA 22904 (USA)
E-mail: dlg9s@virginia.edu
J. Seager, Dr. S. Egorov
University of Virginia, Department of Chemistry
McCormick Road, Charlottesville, VA 22904 (USA)
E-mail: sae6e@virginia.edu

[**] We would like to thank Frans Leermakers for the use of SFBOX, software based on the Scheutjen–Fleer lattice model. Moreover, we appreciate the financial support received from the University of Virginia in particular NanoSTAR (http://nanostar.virginia.edu) and the American Chemical Society (ACS PRF-53934ND6).

Supporting information for this article is available on the WWW under http://dx.doi.org/10.1002/anie.201500906.

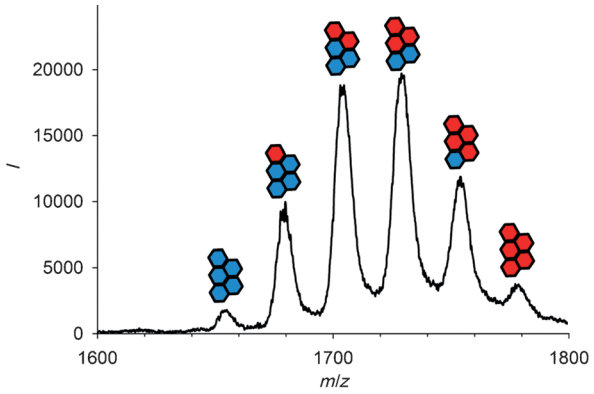

Figure 1. MALDI spectrum of the Ag_6L_5 fragment from Ag nanoparticles functionalized with DDT and its deuterated analogue [D_{25}]DDT. Depicted above the spectrum are the number of DDT (blue) and [D_{25}]DDT (red) ligands on a fragment corresponding to each MALDI peak.

the degree of ligand phase separation. Random mixing is anticipated for the DDT/[D_{25}]DDT monolayer; thus, its frequency distribution coincides with the binomial distribution in Figure 2b.

Calculations on the volume-fraction profiles from the Scheutjen–Fleer self-consistent mean-field lattice model (SCF)[10] were used to simulate a theoretical spectrum, which could be compared to that obtained experimentally using MALDI mass spectrometry. It is appropriate to employ the SCF adsorption theory to model ligand interactions on silver as the SAM has a graft density approaching 5 ligands/nm^2,[11] equating to the concentrated brush regime where the mean-field approximation applies.[12] Further approximations were made to speed up computations. Although silver nanoparticles are faceted icosahedrons,[13] the particle geometry was modeled as a pixelated sphere, permitting analyses to be carried out in Cartesian coordinates. Moreover, each ligand monomer fills a lattice site of constant size, thus ligand and solvent monomers are the same size in the simulations. To this end, three species are considered: the solvent and two chemically distinct ligands whose effective interaction is modeled by a Flory parameter, χ. The particle diameter was set to 20 lattice units, equivalent to the actual particle size of 3–4 nm,[14] and the number of monomers in a ligand were equated to the same number on the lattice; thus, dodecanethiol and butanethiol, respectively, are twelve and four lattice monomers long. An additional parameter is the dimensionless surface coverage θ which we set to $\theta = 0.44$, equating to full monolayer coverage. The adsorbed ligand concentrations in the simulations were varied by changing the ratio of the two ligands on the surface. Subsequently, the resulting SCF calculations were then compared to the MALDI results with a similar ligand ratio. The SCF calculations were carried out subject to the constraints of the minimization of the free energy and the conservation of mass. The resulting equilibrium volume-fraction profiles were determined by solving the polymer diffusion equation for each species with the appropriate boundary conditions, where each ligand was pinned and allowed to move around the interface. The current SCF formalism does not account for inter-chain crystallization known to occur in alkane thiols with carbon lengths $C \geq 10$–12.[15] The agreement between theory and experiment below indicate that although the effects of inter-chain crystallization may be present, their influence is minimal on the random mixing between DDT/[D_{25}]DDT and phase separation between monolayers of DDT and much shorter butanethiol(BT) chains.

To simulate a MALDI spectrum, statistical analysis was performed on the monomer of each ligand pinned at the interface to mimic tracking of the Ag_6L_5 fragment. In particular, the two species of ligands on the fragment result in six peaks on a MALDI spectrum, representing the six possible binomial combinations. To simulate this distribution, a histogram was calculated from the probability, $P_{w,i}$, which was computed by summing the probability at each lattice space that was treated locally as a binomial of the six possible ligand combinations as weighted by the local volume fractions of the pinned monomers. The probability, $P_{w,i}$, is shown in Equation (1), where $i = 0 \ldots n$, is the number of fragments out of a total of $n = 5$ fragments of the first ligand species; this species is DDT. The ligand volume fraction is ϕ and the subscript B denotes tracking of the other ligand species; the total interfacial concentration of DDT and species B are considered when ϕ includes the subscript T. The subscript, $k = 1\text{M}$, is an index for each ligand site for a total number of sites M. Equation (3) displays the SSR, which is determined by squaring and summing the residual, $P_{w,i} - P_{bi,i}$, where $P_{bi,i}$ is the binomial distribution in Equation (2).

$$P_{w,i} = \frac{\sum_{k=1}^{M} \left(\phi_{\mathrm{DDT}_k} + \phi_{\mathrm{B}_k}\right)^n \binom{n}{i} \phi_{\mathrm{DDT}_k}^{i} \phi_{\mathrm{B}_k}^{n-i}}{\sum_{k=1}^{k=M} \left(\phi_{\mathrm{DDT}_k} + \phi_{\mathrm{B}_k}\right)} \tag{1}$$

$$P_{bi,i} = \binom{n}{i} \phi_{\mathrm{DDT}_T}^{i} \phi_{\mathrm{B}_T}^{n-i} \tag{2}$$

$$SSR = \sum_{i=1}^{n} \left(P_{w,i} - P_{bi,i}\right)^2 \tag{3}$$

To connect experiment and theory, we analyzed the MALDI distributions of monolayers composed of DDT, an alkane thiol with 12 carbons, in combination with butanethiol (BT), a shorter alkane thiol with four carbons, or deuterated dodecanethiol [D_{25}]DDT. One purpose is to use MALDI and SCF to establish the existence of phase separation for the DDT/[D_{25}]DDT- and DDT/BT-mixed monolayers, which should result in well-mixed or striped monolayers, respectively. Well-mixed monolayers are anticipated for the DDT and [D_{25}]DDT coated nanoparticles as a result of the chemical similarity of the ligands. Striped monolayers should result from the microphase segregation of DDT and BT, promoted by an increase in the conformational entropy of the longer ligand. A Flory parameter of $\chi_{\mathrm{CH_2}} = 0$ was chosen to model the athermal interaction between the methyl and methylene groups of DDT, [D_{25}]DDT, BT, and a simulated ethanol solvent. The Flory parameter between the hydroxy group of ethanol and the methyl and methylene groups of the ligands was set at $\chi_{\mathrm{CH_2/OH}} = 2.0$.

Figure 2 shows the comparison between the MALDI spectra for the 50/50 mol% DDT/[D_{25}]DDT and DDT/BT monolayers and the corresponding SCF predictions. The SCF images display the locations for DDT in blue and the

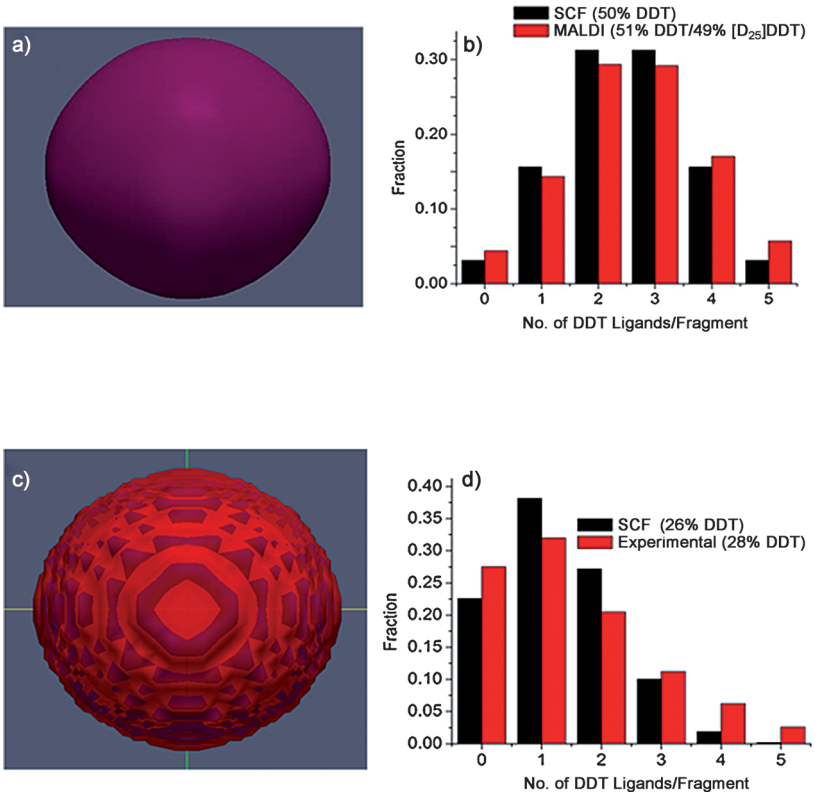

Figure 2. Comparison between the MALDI mass spectra and SCF predictions. a) SCF image of well-mixed monolayer with simulated dodecanethiol (DDT) in blue and [D_{25}]DDT in red, colors mix as purple. b) MALDI spectra for the well-mixed DDT/[D_{25}]DTT monolayer functionalized Ag nanoparticles and the corresponding SCF prediction. c) SCF image of the striped nanoparticle with simulated DDT in blue (overlapping with red to give purple) and butanethiol (BT) in red. d) MALDI spectra for microphase separated DDT/BT monolayer functionalized Ag nanoparticles and corresponding SCF prediction. For clarity, error bars are not shown.

opposing ligand in red. Thus, the color of the well-mixed monolayer is uniform, that is, one color, denoting random mixing in Figure 2a. This random mixing is supported by the correspondence between the MALDI and SCF spectra for DDT and [D_{25}]DDT in Figure 2b where random mixing is indicated by the higher probability of having silver fragments with either two or three DDT ligands. In contrast, Figure 2c illustrates microphase separation and striped nanoparticle formation for semimiscible ligand mixtures, which is also supported by the agreement between the simulated and experimental spectra for DDT and BT in Figure 2d.

Although the error in the MALDI data is not shown in Figure 2 for clarity, variance in the data is due to random fluctuations in ligand ordering and error resulting from small variations in the triggering time or accelerating voltage in the MALDI system. Error in peak alignment is typically measured to be on the order of 0.1%,[16] which is anticipated to be smaller than random error. Hence, the standard deviation (σ) resulting from random fluctuations was estimated by comparing the spectra of the well-mixed monolayer DDT/[D_{25}]DDT to the binomial distribution through $\sigma = [SSR/(j-1)]^{1/2}$ for $j =$ 84 peaks yielding $\sigma = 0.04$, indicating that the peaks derived experimentally from MALDI mass spectrometry deviate from those calculated using SCF by 4%.

A plot of the SSR in Figure 3 provides another measure of ligand phase separation by quantifying the deviation from random mixing. To this end, we employed a one-step reaction scheme[14] to synthesize silver nanoparticles with monolayers of DDT and [D_{25}]DDT as well as DDT with BT to detect of the effect of differences in the carbon chain length in the ligands, ΔC, on phase separation over a range of interfacial concentrations. As a result of their chemical similarity, low SSR values from SCF and MALDI are anticipated for the DDT/[D_{25}]DDT monolayer with $\Delta C = 0$. For example, the SSR values from SCF are negligible ($SSR \approx 10^{-19}$, i.e., smaller than the relative error caused by rounding in floating-point arithmetic). Thus, the SCF calculation for favorably interacting, similar-sized ligands converges to the binomial distribution in Equation (2), supporting our choice of this distribution to model a well-mixed monolayer. The experimental SSR values for the DDT/[D_{25}]DDT monolayer are low, on the order of 10^{-3}–10^{-2}, similar to values obtained with MALDI for randomly-mixed monolayers by Cliffel and co-workers.[8] The SSR values should increase with monolayers of DDT and BT with $\Delta C = 8$, as microphase separation is expected to occur for alkane thiol mixtures with a sufficient chain-length difference through gains in mixing entropy.[5] The SSR values obtained from MALDI experiments for DDT/BT monolayers increase 10-fold in comparison

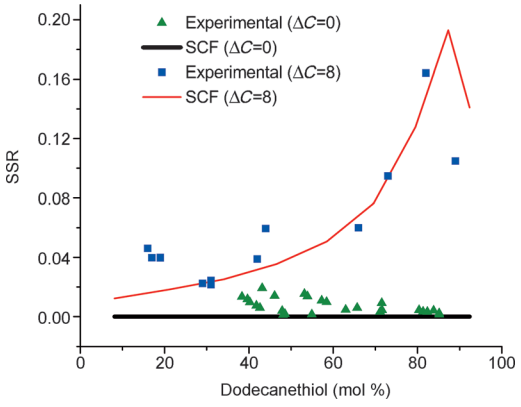

Figure 3. Comparison between experimental and theoretical SSR values from MALDI experiments and SCF calculations.

to the well-mixed case ($10^{-1} \gg 10^{-2}$). The theoretical SSR value matches the trends and magnitude of the MALDI SSR, indicating good agreement between experiment and theory.

Through this work, we have demonstrated the ability to quantify and predict the phase separation of alkane thiols on Ag nanoparticles using MALDI and SCF as a function of both

ligand concentration and carbon-chain-length difference. These results indicate that when pairing DDT with either its deuterated analogue [D_{25}]DDT or BT the SAM morphology progressed from a random ligand distribution to an intermediate degree of phase separation. We anticipate these methods will find utility in the design of nanomaterials with properties arising from phase-separated SAMs as they offer an inexpensive, high-throughput method for the measurement of ligand phase separation in nanoparticle systems.

Experimental Section

Silver nitrate (99.9999% purity), sodium borohydride (99.99%), 1-dodecanethiol (≥98%), 1-butanethiol (99%), and trans-2-[3-(4-*tert*-Butylphenyl)-2-methyl-2-propenylidene]malononitrile (DCTB, ≥99.0%) were purchased from Sigma–Aldrich. Absolute ethanol and toluene (ACS reagent grade) were purchased from Fisher Scientific. Deuterated 1-dodecanethiol ([D_{25}]dodecanethiol, 98.9 atom% deuterium) was purchased from C/D/N Isotopes. All reagents were used with no further purification. Ultrathin (<3 nm) carbon film on 400 mesh copper holey carbon grids for TEM imaging were purchased from Ted Pella.

Mixed self-assembled monolayer Ag nanoparticles were synthesized by our direct method with the molar ratio of thiol ligand to silver nitrate held constant at 12 throughout all syntheses while varying the individual thiol concentrations in a given pair.[14] Silver nitrate was maintained at 0.5 mM in ethanol in all reactions and sodium borohydride was kept at a 12-fold excess at 6 mM. After initiation of the reaction by combining the reagents, the mixture was stirred for 30 min and then transferred to centrifuge tubes and centrifuged at 12000 rpm for 20 min. Following centrifugation, the supernatant was decanted and replaced with fresh ethanol. Subsequently the nanoparticles were redispersed by sonication and were again centrifuged. This was repeated three times and after the third and final centrifugation the nanoparticles were redispersed in toluene.

Nanoparticle samples were characterized using TEM and MALDI mass spectrometry. All TEM images were taken with an FEI Titan at an accelerating voltage of 300 kV. A drop-mounting method was used to prepare TEM samples. A TEM grid was held within self-closing tweezers and a pipette used to place a drop of nanoparticle solution onto the grid. A small piece of filter paper was used to wick away extra solvent and the grid was dried for at least one hour. Determination of nanoparticle size was performed using automated routines built into ImageJ software. MALDI measurements were performed on a Bruker MicroFlex. To prepare solutions for spotting onto a MALDI plate, *trans*-2-[3-(4-*tert*-butyl-phenyl)-2-methyl-2-propenylidene]malononitrile (DCTB; 0.025 g) were dissolved in 1 mL of nanoparticle solution. 100 μL of this solution was spotted per well of a standard ground-steel Bruker MALDI plate. Laser power was kept at 40% across all measurements with the detector operated in linear mode. Individual ion counts were calculated by integrating the area under the peak of interest using the trapezoid rule; in every case, these values were calculated for each ion of interest in the Ag_6L_5 series.

Keywords: mass spectrometry · nanoparticles · nanotechnology · self-assembly · statistical thermodynamics

How to cite: *Angew. Chem. Int. Ed.* **2015**, *54*, 6479–6482
Angew. Chem. **2015**, *127*, 6579–6582

[1] W. Brullot, R. Strobbe, M. Bynens, M. Bloemen, P.-J. Demeyer, W. Vanderlinden, S. De Feyter, V. K. Valev, T. Verbiest, *Mater. Lett.* **2014**, *118*, 99–102.

[2] V. Camarchia, A. Chiolerio, M. Cotto, J. Fang, G. Ghione, P. Pandolfi, M. Pirola, R. Quaglia, C. Ramella, *Org. Electron.* **2014**, *15*, 91–98.

[3] E. Jeong, G. Jung, C. Hong, H. Lee, *Arch. Pharmacal Res.* **2014**, *37*, 53–59.

[4] N. Dutta, D. Green, *Langmuir* **2010**, *26*, 16737–16744.

[5] a) S. A. Egorov, *Soft Matter* **2012**, *8*, 3971–3923; b) C. Singh, P. Ghorai, M. Horsch, A. Jackson, R. Larson, F. Stellacci, S. Glotzer, *Phys. Rev. Lett.* **2007**, *99*, 226106.

[6] a) A. M. Jackson, J. W. Myerson, F. Stellacci, *Nat. Mater.* **2004**, *3*, 330–336; b) A. M. Jackson, Y. Hu, P. J. Silva, F. Stellacci, *J. Am. Chem. Soc.* **2006**, *128*, 11135–11149; c) A. Centrone, Y. Hu, A. M. Jackson, G. Zerbi, F. Stellacci, *Small* **2007**, *3*, 814–817; d) See Ref. [5b]; e) R. P. Carney, G. A. DeVries, C. Dubois, H. Kim, J. Y. Kim, C. Singh, P. K. Ghorai, J. B. Tracy, R. W. Murray, S. C. Glotzer, F. Stellacci, *J. Am. Chem. Soc.* **2008**, *130*, 798–799; f) G. A. DeVries, F. R. Talley, R. P. Carney, F. Stellacci, *Adv. Mater.* **2008**, *20*, 4243–4247; g) Y. Hu, O. Uzun, C. Dubois, F. Stellacci, *J. Phys. Chem. C* **2008**, *112*, 6279–6284; h) K. Nakata, Y. Hu, O. Uzun, O. Bakr, F. Stellacci, *Adv. Mater.* **2008**, *20*, 4294–4299; i) A. Verma, O. Uzun, Y. H. Hu, Y. Hu, H. S. Han, N. Watson, S. L. Chen, D. J. Irvine, F. Stellacci, *Nat. Mater.* **2008**, *7*, 588–595; j) J. J. Kuna, K. Voïtchovsky, C. Singh, H. Jiang, S. Mwenifumbo, P. K. Ghorai, M. M. Stevens, S. C. Glotzer, F. Stellacci, *Nat. Mater.* **2009**, *8*, 837–842; k) A. Ghosh, S. Basak, B. H. Wunsch, R. Kumar, F. Stellacci, *Angew. Chem. Int. Ed.* **2011**, *50*, 7900–7905; *Angew. Chem.* **2011**, *123*, 8046–8051; l) X. Liu, Y. Hu, F. Stellacci, *Small* **2011**, *7*, 1961–1966; m) C. Singh, Y. Hu, B. P. Khanal, E. R. Zubarev, F. Stellacci, S. C. Glotzer, *Nanoscale* **2011**, *3*, 3244–3250; n) O. Uzun, Y. Hu, A. Verma, S. Chen, A. Centrone, F. Stellacci, *Chem. Commun.* **2008**, 196–198; o) M. Moglianetti, Q. K. Ong, J. Requera, K. M. Harkness, M. Mameli, A. Radulescu, J. Kohlbrecher, C. Jud, D. Svergun, F. Stellacci, *Chem. Sci.* **2014**, *5*, 1232–1240.

[7] Y. Cesbron, C. P. Shaw, J. P. Birchall, P. Free, R. Lévy, *Small* **2012**, *8*, 3714–3719.

[8] K. Harkness, A. Balinski, J. McLean, D. Cliffel, *Angew. Chem. Int. Ed.* **2011**, *50*, 10554–10559; *Angew. Chem.* **2011**, *123*, 10742–10747.

[9] P. Casuso, P. Carrasco, I. Loinaz, G. Cabanero, H. J. Grande, I. Odriozola, *Soft Matter* **2011**, *7*, 3627–3633.

[10] a) J. M. H. M. Scheutjens, G. J. Fleer, *J. Phys. Chem.* **1979**, *83*, 1619–1635; b) J. M. H. M. Scheutjens, G. J. Fleer, *J. Phys. Chem.* **1980**, *84*, 178–190; c) G. J. Fleer, M. A. Cohen Stuart, J. M. H. M. Scheutjens, T. Cosgrove, B. Vincent, *Polymers at Interfaces*, Chapman and Hall, New York, **1993**.

[11] A. Janz, A. Köckritz, L. Yao, A. Martin, *Langmuir* **2010**, *26*, 6783–6789.

[12] P. G. De Gennes, *Scaling Concepts in Polymer Physics*, Cornell University Press, Ithaca, **1979**.

[13] J. A. Ascencio, C. Gutiérrez-Wing, M. E. Espinosa, M. Marín, S. Tehuacanero, C. Zorrilla, M. José-Yacamán, *Surf. Sci.* **1998**, *396*, 349–368.

[14] Z. Farrell, C. Shelton, C. Dunn, D. Green, *Langmuir* **2013**, *29*, 9291–9300.

[15] a) S. Egorov, H. Hsiao-Ping, A. Milchev, K. Binder, *Soft Matter* **2015**, *11*, 2604–2616; b) K. G. Pradip, S. C. Glotzer, *J. Phys. Chem. C* **2007**, *111*, 15857–15862; c) W. Mar, M. L. Klein, *Langmuir* **1994**, *10*, 188–196; d) F. A. M. Leermakers, M. A. Cohen-Stuart, *Phys. Rev. Lett.* **1996**, *76*, 82–85.

[16] M. B. Tracy, H. Chen, D. M. Weaver, D. I. Malyarenko, M. Sasinowski, L. H. Cazares, R. R. Drake, O. J. Semmes, E. R. Tracy, W. E. Cooke, *Proteomics* **2008**, *8*, 1530–1538.

Received: January 30, 2015
Revised: February 22, 2015
Published online: April 16, 2015

